Brazilian Journal of Geophysics, **42** (2024), 2, 1–16
Brazilian Geophysical Society
ISSN 2764-8044
DOI 10.22564/brjg.v42i2.2319

# A TWO-DIMENSIONAL AMPLITUDE STUDY OF TRUE-AMPLITUDE TIME MIGRATION AND TIME REMIGRATION – 2.5-D SYNTHETIC EXAMPLES

Carlos Augusto Sarmento Ferreira [1*], Karina Palheta Gomes [2] and Alexandre de Souza Oliveira Oliveira [3]

[1]Agência Nacional de Mineração - ANM, Cuiabá, MT, Brazil
[2]Universidade Federal do Acre - UFAC, Rio Branco, AC, Brazil
[3]Observatório Nacional - ON, Rio de Janeiro, RJ, Brazil

*Corresponding author: carlos.ferreira@anm.gov.br

**ABSTRACT.** In this synthetic study, we present semi-automatically picked true-amplitude comparisons after time migration and time remigration (Tygel et al., 1996; Oliveira et al., 2023). Since the examples considered are synthetic, emphasis is put on the generally disregarded dimensional aspects of the amplitudes that are modeled to simulate compressional-only seismic data when using a Kirchhoff approximation. By bearing in mind in this work that theoretical amplitudes work as "densities", we show that when comparisons of true-amplitude weighted diffraction-stack time migration and weighted isochrone-stack time remigration are performed, in order to "correct" the dimensions involved, certain multiplicative physical constants must come into play and that must be effectively dealt with for plotting reasons.

**Keywords:** Amplitude density; dimensional scaling factors; synthetic seismic modeling; weight functions; Kirchhoff approximation

## INTRODUCTION

Seismic reflection amplitudes are one of the most important parameters to be considered in data processing since, besides resolution, it may contain fluid information, mainly gas content, typically considered in amplitude-versus-offset (AVO) studies. Classically, it has been documented that it is affected by a sort of factors (Sheriff, 1975), including source strength, directivity, coupling, multiples, spherical divergence etc. But, since, according to O'Doherty and Anstey (1971), "*modern seismic recording instruments allow precise measurements of the amplitude of reflected signals, intuitively it is expected that this amplitude information could be used to increase our knowledge of the physical properties of the reflecting Earth*". In this sense, along the years, seismic migration (either in depth or in time) has been developed as true-amplitude to assess measures of angle-dependent reflection coefficients of seismic data picked along key reflectors. This allows one to define an approximated image of the subsurface geology as well as assess its physical properties in an inversion procedure, like vector-weighted diffraction stack (Tygel et al., 1993).

In this paper, we report on the comparison of semi-automatically picked amplitudes along synthetic reflectors derived from a Kirchhoff-type time migration and time remigration, following the methodology presented in Oliveira et al. (2023) for true-amplitude imaging in the time domain. In this study, due to the nature of definition for amplitudes, reflection coefficients and transmission loss factors, we investigate the "density" nature of modeled seismic reflections. This is because when modeling synthetic seismic data in 2-D or in 2.5-D, one must notice that amplitudes in these domains are types of "densities" derived from 3-D amplitudes of 3-D sources. In this sense, square root of out-of-plane factors come into play and must adequately be included or multiplied to, e.g., in the part of the total amplitude that contains the geometrical-spreading factors.

When considering true-amplitude imaging (Hubral et al., 1996; Tygel et al., 1996), weights are applied in migration or demigration procedures to grant the best possible amplitudes between one process and another. This is the raytracing-based general approach of reflection imaging proposed by Hubral, Tygel and Schleicher in the 90s (see References). Specifically, in remigration and configuration transforms, a cascading of migration/demigration weight functions are applied in succession to grant a diffraction stack or isochrone stack solution (Tygel et al., 1996). Martins (2001) reduced this general approach of Tygel et al. (1996) to the 2.5-D geometry for a single-stack solution and specified the weight functions to be used in this domain. In Oliveira et al. (2023), migration and remigration are performed in the time domain using weights also in time as well, but only the kinematic aspects were considered and their respective imaging results. Our aim here is to consider the dynamic aspect of this theory in the time domain and focus on amplitudes.

In 2.5-D raytracing, out-of-plane factors are naturally incorporated in amplitudes due to the solutions of the ray equations (Bleistein, 1986). But when reducing a two-fold to a one-fold integral in the high-frequency approximation using the method of stationary phase, the reciprocal of the square root of another well-known out-of-plane factor is also incorporated in amplitudes – i.e., more specifically, in the geometrical-spreading factor. Therefore, in synthetic modeling, beyond reflection coefficients and amplitude losses due to transmission (which are dimensionless quantities), there appears an "amplitude density" factor with dimension of $[s^{1/2}/m^2]$ ($s$ for seconds and $m$ for meters). After stack integration along each possible reflector by means of a multiplication by a differential $dx$, the result is that seismic data are dimensionally equivalent to some "*value* X *something*" (in which "*something*" has a dimension of $[s^{1/2}/m]$), which is still a "density" value. This is the starting point for the following considerations in this work. For migration and remigration in the time domain – each process performed following their specific sequence –, their respective weight functions are scalable, each one with a proper own dimension and multiplied by another differential $dx$. So far (and for plotting purposes only), nothing new or incorrect is done that is unknown, such that kinematically all output sections (seismic and migrated) are correct. But if one picks several or some amplitudes along one specific reflector and tries to compare them, it will be noticed that their values are proportional but not with the same magnitude. Thus, our claim is that, for a fair comparison, some sort of dimensional factor must multiply each picked amplitude to equalize their magnitudes and label the term "true-amplitude" in a reasonable way.

It is important to state that we mean no milestone in amplitude studies with the results and proofs shown in this work. Our only intention was to clarify and understand common perceptions in seismic modeling and migration studies, to which we hope to have contributed somehow in a very ad hoc manner. We are aware that scaling factors are part of modeling, either physical or numerical. In this work we will show the results of semi-automatic amplitude picking comparisons recovered from two 2.5-D synthetic seismic datasets (simple and complex) and discuss their physical interpretation and possible applications.

This work is organized as follows: in the first section we discuss the methodology regarding the idea of viewing amplitudes as densities in 2-D synthetic studies. The weight function for the time remigration is introduced according to a recent study described in Oliveira et al. (2023). Due to the fact that comparisons existing among different picked amplitudes are the main topic of this paper, we decided to allocate these results in a separate section. Therefore, in the second section we present the synthetic datasets that were used in this paper, which include unmigrated, migrated, undermigrated and remigrated results. Then, the third section follows regarding results and discussions, in which we examine the main pickings obtained after considering cases of constant velocity medium (with and without lateral velocity variations) for a single reflector and the results obtained from a stratigraphic model (with lateral velocity variation), the latter one representative of the pre-salt geology of any Brazilian East Margin offshore basins. After our conclusions, a brief discussion about remigration is appended in order to show some aspects of the theory in the time domain.

## METHODOLOGY

Let us consider that a set of 2-D synthetic datasets is available for imaging processing in the time domain. These synthetics may include common-offset sections that were specifically sorted to this visual geometry so that prestack or poststack procedures are possible choices for any subsequent workflow. Then, some amplitude-preserving and kinematic-only imaging procedures are generated upon these datasets: weighted-Kirchhoff time migration (Schleicher et al., 1993) and unity-weight Kirchhoff time migration, respectively. Suppose then that at least two velocity fields are also available for processing, each one with a different degree of accuracy with respect to each other regarding their stacking values. Also, lateral velocity gradients issues are considered admissible to these fields.

When an accurate RMS velocity field is available, Kirchhoff time migration correctly locates and focus amplitudes towards their pseudo-depth positions. In this sense, diffractions are also collapsed. If certain weights are then applied during migration, primary reflection amplitudes may be corrected for some propagation losses, such as geometrical spreading (Schleicher et al., 1993). When this is not so, it can be said that the final image is only kinematically correct. This issue of inaccurate velocity values in Kirchhoff time migration has been recognized for years as source of poor imaging. And when velocity variation is not only function of stratigraphic layering, for time migration focusing of reflections and collapsing of diffractions become an incomplete seismic imaging. Now consider the possibility of using a process in which it is possible to complete the action of focusing and collapsing of reflections and diffractions, respectively. This imaging procedure is called remigration (Hubral et al., 1996; Tygel et al., 1996) and makes use of two velocity fields to continue the action as a residual migration (Fomel, 2003).

Common to all these procedures commented so far is the treatment of amplitudes. Moving one amplitude sample updip or downdip following these imaging operations should preserve, in principle, the magnitude of the event, simply because these are just being moved somewhere. But migration itself modifies the amplitude content of the event at least in the spectral domain, differentiating dipping and horizontal reflections. In the realm of 3-D real seismic data, it is considered that this problem is far complicated. Therefore, let us focus on 2-D synthetics and study the nature of its dimension and what happens to amplitudes.

## Kirchhoff time remigration

As described in Oliveira et al. (2023), in the examples that follows a tilde symbol ("$\sim$") over functions and variables refer to the output space, including spatial positions, time coordinates and velocities. The remaining variables and functions without tildes refer to the input space, also including spatial positions, time coordinates and velocities. Examples of datasets belonging to input space are the seismic data $U(\xi, t)$, velocity field $v_{RMS}(x, \tau)$ and time-migrated section $I(x, \tau)$, respectively. For a brief description of time remigration theory and its domain, see Appendix A.

The input and output spaces both consider an arbitrary 2-D single-fold measurement configuration of point sources and receivers distributed along the Earth surface, the location of them described by parameter $\xi$, which varies in $A$, called migration aperture. Therefore, for each point $(\tilde{x}, \tilde{\tau})$ in the output, time-remigrated section to be simulated, the stack result $\tilde{I}(\tilde{x}, \tilde{\tau})$ is obtained by a weighted stack of the input data, represented by the integral operator defined by Oliveira et al. (2023) (Appendix A), in which $I(x, \tau)$ is the input, time-migrated (analytic) seismic section that is to be weighted by $K_{RM}^{(2.5D)}(x; \tilde{x}, \tilde{\tau})$ and then summed up along the stacking line or inplanat $\tau = t_{RM}(x; \tilde{x}, \tilde{\tau})$ (Tygel et al., 1996).

Both functions are dependent on the point $(\tilde{x}, \tilde{\tau})$ where the stack is to be placed and on the variable $x$ that specifies the location of the traces being summed in the stack. Moreover, $A$ denotes the spatial limited aperture of the stack, the range of midpoints in a common-offset gather available in the time-migrated input section, $I(x, \tau)$. The stacking line $\tau = t_{RM}(x; \tilde{x}, \tilde{\tau})$ is defined by the kinematics of the operation and the weight function $K_{RM}^{(2.5D)}(x; \tilde{x}, \tilde{\tau})$ is determined by the desired amplitude behavior.

### Weight function

The remigration weight function used in the examples is the product of 2.5-D migration and demigration weight functions (Tygel et al., 1996; Martins, 2001; Oliveira et al., 2023). Thus, in the time domain we consider approximately:

$$K_{RM}^{(2.5D)}(x; \tilde{x}, \tilde{\tau}) = \frac{\sqrt{2}}{2} \frac{\tilde{\tau}}{v_{RMS}^{3/2}} \sqrt{\frac{1}{\tilde{t}_S} + \frac{1}{\tilde{t}_G}} \times \left(\frac{1}{\tilde{t}_S} + \frac{1}{\tilde{t}_G}\right) \frac{1}{(t_1 + t_2)} \sqrt{\frac{1}{t_1} + \frac{1}{t_2}}. \quad (1)$$

where $\tilde{t}_S$ and $\tilde{t}_G$ are double square roots (DSRs) for source and receivers in the output domain for coordinate $(\tilde{x}, \tilde{\tau})$ and velocity $\tilde{v}_{RMS}$, while $t_1$ and $t_2$ are DSR equations in the input domain, together with $v_{RMS}$ in this input domain. Dimensionally, this weight function is expressed in $[s^{(1/2)}/m^{(3/2)}]$ units.

Apart from the form of the weight function in (1), a dimensionless stretch factor and a term regarding "local dip" at the reflector in the time domain may also be multiplied when referred. Other terms that may be multiplied in (1) are square roots of absolute values of determinants of Hessian matrices or, in 2.5-D, curvatures of diffraction traveltimes for points in the input and output domains (Tygel et al., 1998; Martins, 2001).

Physically, weight function (1) is completely represented by kinematic parameters belonging to the input $(t_1, t_2, v_{RMS})$ and output $(\tilde{\tau}, \tilde{t}_S, \tilde{t}_G)$ spaces, respectively. In this sense, the layout of Equation (1) just displays the product of each contribution relating chained processes of migration and demigration (Oliveira et al., 2023).

We do not specify the weight functions for the weighted diffraction-stack migration because they are well-known in the literature (e.g., Schleicher et al., 1993). Also, one unity weight is used for the kinematically only Kirchhoff migration cases.

With the weights defined in this way, we will show that the remigration process "pulls" the undermigrated amplitudes to the true-migrated ones, considering, of course, limitations related to aperture issues and border effects or even picking problems.

### Apertures

In principle, no restrictions will be imposed to apertures. Only analytical cases are considered, using ideas of offset-continued traveltime surfaces already studied in the literature (e.g., see Fomel, 2003). To other concerns regarding aperture issues, see a brief discussion in Appendix A.

### Input data available for picking

All seismic sections available for amplitude picking in this paper are space-time equivalent. Therefore, each picked amplitude profile must have the same length.

Each section shall be considered in the following order:

- An input seismic section (common-offset).
- A diffraction-stacked, weighted, time-migrated section (Schleicher et al., 1993).
- A diffraction-stacked, unity-weight, time-migrated section.
- A time-remigrated section, in which for this latter the input section is one undermigrated, diffraction-stacked section using an inaccurate velocity model.

Besides the issue of true amplitudes in time domain, we claim in the comparisons the behavior of each procedure according to the ones already described in the literature in terms of magnitude, losses (geometrical spreading), and polarity issues.

### Amplitude considerations

Let us simplify some definitions and state that 3-D sources that gave rise to 2.5-D amplitudes in our examples present no issues regarding directivity or coupling. Also, no attenuating properties of the medium are considered, only geometrical spreading and reflection coefficients are regarded. Transmission losses across interfaces are not present in our examples.

Impedance contrasts are present in both synthetic datasets. In some sense, however, they may be taken as optional, since reflections derived from their models are essentially the final result of an analytic integration along mathematical reflectors and may even be set to unity when referred to. As a result, picked amplitudes will, in principle, be proportional to angle-dependent reflection coefficients.

In the following we consider each dimensional contributions of each numerical operation in the time domain in the sequence: modeling, weighted-Kirchhoff migration, unity-weight Kirchhoff migration and Kirchhoff remigration. Each mathematical operation is responsible for a dimensional contribution to amplitude values, according to the table below.

Each entry in Table 1 in the column "Contribution (dimension)" represents one contribution to each amplitude "density". In their final form, these contributions are the result of the multiplication of several factors that constitute one weight function in each mathematical operation, either modeling, migration, or remigration. The last factor that contributes dimensionally is the differential $dx$ of each operator. Therefore, each result listed in the column "Amplitude ("density")" is the term regarded as "amplitude" that is inserted into each final time-migrated or time-remigrated seismic section under the peak of each wavelet signal. The scaling factors derived for each example are the ones that are then multiplied to each picked event in the examples, turning their amplitudes dimensionless.

In each example, a peak of a reflected and migrated event will be semi-automatically chosen to compare its value with the peak in the input seismic section and in the time-migrated and time-remigrated output sections. These amplitudes will then be scaled accordingly to their "density" nature in the manner assessed in this paper and listed in Table 1.

It must be noticed that peak amplitudes are selected in order to preserve the idea of higher value. Another possible idea is to use the envelope of the analytical signal, since this is an attribute that is related to the maximum reflection and normally preserves the lateral continuity of seismic events. Also, there may appear, in some cases, issues related to change of polarity, a feature that must be adequately cared and carefully considered. A manual picking, in these cases, may be able to resume this kind of difficult.

## EXAMPLES

In this section, we briefly introduce the synthetic datasets used in this paper. We first introduce the synthetic seismic sections and then their respective migrated results. We consider presenting the datasets in this way because the picking procedure that is the main objective of this paper is realized upon unmigrated and migrated sections. Since the inclusion of lateral velocity variations skews reflections, when dealing with imaging in time, these features must be taken into account, as it is known that automatic picking will face some drawbacks.

We have tested our algorithm in two synthetic datasets. The first one is represented by a common-

**Table 1:** Numerical contribution to amplitudes.

| Numerical Operation | Contribution (dimension) | Amplitude ("density") | Scalling (factor) |
|---|---|---|---|
| Modeling | $\frac{\sqrt{2}}{2}\frac{s^{1/2}}{m^2}\,dx$ | $\frac{\sqrt{2}}{2}\frac{s^{1/2}}{m}$ | $\sqrt{2}\frac{dx}{s^{1/2}}$ |
| Weighted-Kirchhoff | $\frac{\sqrt{2}}{2}\frac{s^{1/2}}{m}s^{1/2}\frac{dx}{m}$ | $\frac{\sqrt{2}}{2}\frac{s}{m}$ | $\sqrt{2}\frac{dx}{s}$ |
| Unity-Kirchhoff | $\frac{\sqrt{2}}{2}\frac{s^{1/2}}{m}\frac{dx}{m}$ | $\frac{\sqrt{2}}{2}\frac{s^{1/2}}{m}$ | $\sqrt{2}\frac{dx}{s^{1/2}}$ |
| Remigration | $\frac{\sqrt{2}}{2}\frac{s}{m}\frac{s^{1/2}}{m^{3/2}}$ | $\frac{\sqrt{2}}{2}\frac{s^{3/2}}{m^{3/2}}$ | $2\frac{dx^{5/2}}{s^{1/2}}$ |

offset section simulated over a single-interface model. The second dataset is given by a common-offset section simulated over a stratigraphic model. Both geometry are specified as $2h = 50$m, where $h$ is the half-offset between sources and receivers.

The main features of each model and its respective data are described below (see Figure 1). Grid parameters for models and data are specified as the total number of samples in each direction: $N_x$, $N_z$, $N_t$ and $N_{traces}$ for each respective domain. Their sampling intervals are denoted by $dx$, $dz$, $dt$. For instance, in our examples we have made use of the following equalities: $N_{traces} = N_x$. We use SI units in all examples, but for numerical procedures, multiples and submultiples are normally considered. A gradient of the order of 0.03 Hz was included for lateral velocity variations in the examples when referred.

### Synthetic datasets

- **Single reflector model**. The first example is represented by a common-offset section derived from a single interface of a syncline model located over a half-space (Figure 1a). Model parameters are $N_x = 400$, $N_z = 200$, $dx = dz = 25$ m, while data parameters are $N_{traces} = 300$, $dt = 8$ms, where trace spacing equals to $dx$ as specified above, as well as source and geophone intervals. For the modeled data seen in Figure 2, the velocity in the layer above the interface is constant and equal to 2.5 km/s. The modeled seismic section in this case contains the typical bowtie pattern of reflections associated with this kind of model. Figure 2 depicts the same modeled seismic section, but with a gradient of 0.03 Hz along the $x-$direction added to the constant velocity. Note the time-skewing present along the range of distances from 4.0 km to 7.5 km in this section due to the presence of velocity gradient.

The time sample indicated for semi-automatic picking in all sections in this first model is $t = 2$ s. Note that in the range of distances 1.0 to 4.0 km, reflections belong to the syncline interval of the model and are far delayed in time as expected, forming the bowtie pattern. These amplitudes were not picked for numerical comparison, and what is expected to be picked along this interval around $t = 2$ s is just negligible numerical noise or null values. In both sections of Figure 2, note also the reflections due to the presence of a discontinuity (i.e., normal fault) in the range of distances 4.0 to 4.4 km, which is a second gap that was introduced in this model, representing a second source of null values of reflection amplitudes.

Of course, the picking procedure will suffer some drawbacks in the range of distances 4.0 to 7.5 km when the gradient case is considered (Figure 2b). This is not a main concern, since we are just comparing methods and we shall show that the picked values in this case are at least proportional and show a common trend, despite some polarity issues. In a future work, this can be remedied with manual picking.

- **Pre-salt model**. The second synthetic example considers one previously model studied in Oliveira and Ferreira (2009), which describes the results of the modeling of a simple 2-D seismic dataset acquired over a representative pre-salt model derived from any of the Brazilian East Margin offshore basins (Figure 1b). The geological model that was constructed to simulate the seismic section seen in Figure 3 with its respective interval velocities is originally made up of four depositional sequences: (I) basement (6.5 km/s); (II) pre-salt section (4.5 km/s); (III) salt layer (5.5 km/s); and (IV) the Tertiary-Upper Cretaceous section, with a constant velocity gradient given by $v(z)$. For the same model in the example used in this work, some intervals of its velocity field were updated to include lateral velocity variations in the Cretaceous section and in the SAG/rift section and then transformed to the time domain. The model parameters for this case are $N_x = 720$, $N_z = 160$, $dx = dz = 50$m, whereas data parameters are $N_{traces} = N_x$, $N_t = 1750$ and $dt = 4$ ms.

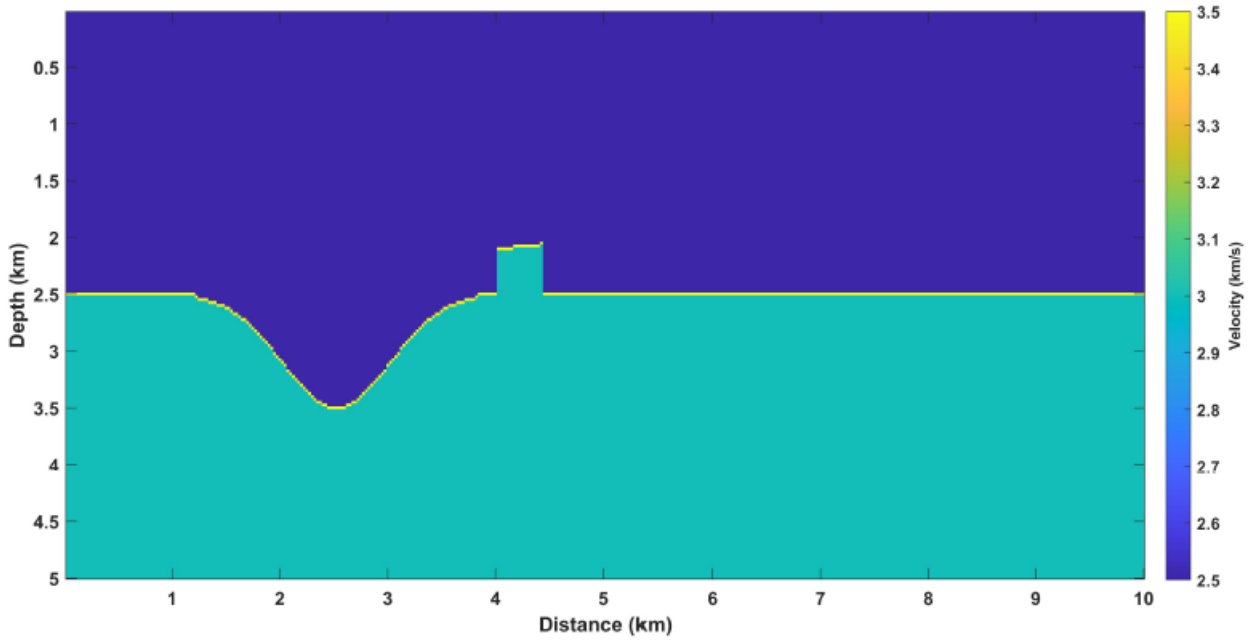


(a) Constant velocity model.

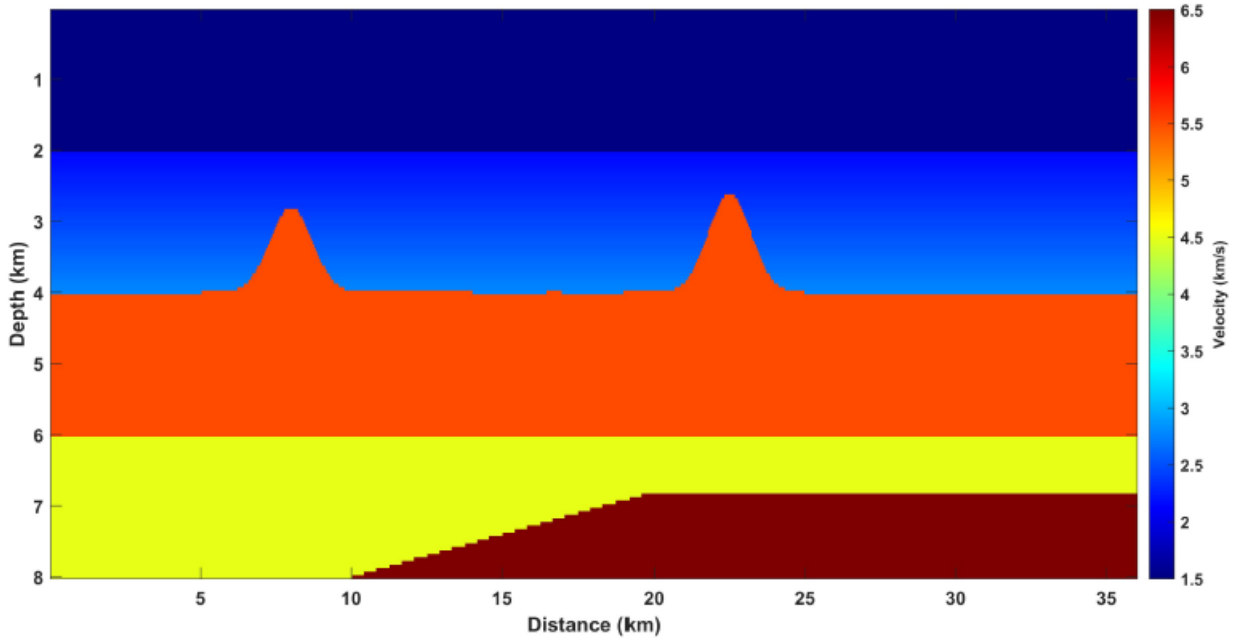


(b) Pre-salt model.

**Figure 1:** Geological models with interval velocities used in the synthetic tests. (a) Velocity is constant in the first layer and equal to 2.5 km/s. The velocity below the interface is set to 3.0 km/s. A second example for this model considers the existence of a gradient of 0.03 Hz in the $x-$direction in the first layer. (b) Pre-salt model considered in Oliveira and Ferreira (2009).

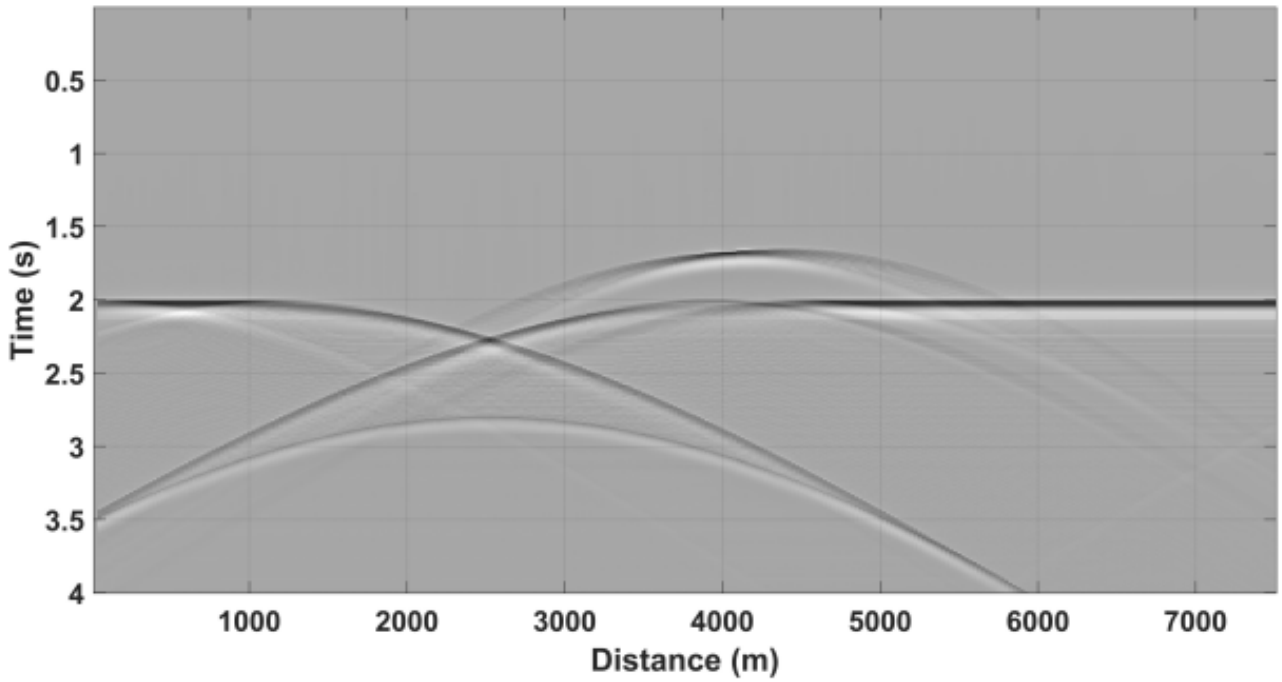


**(a)** Velocity is constant in the first layer and equal to 2.5 km/s.

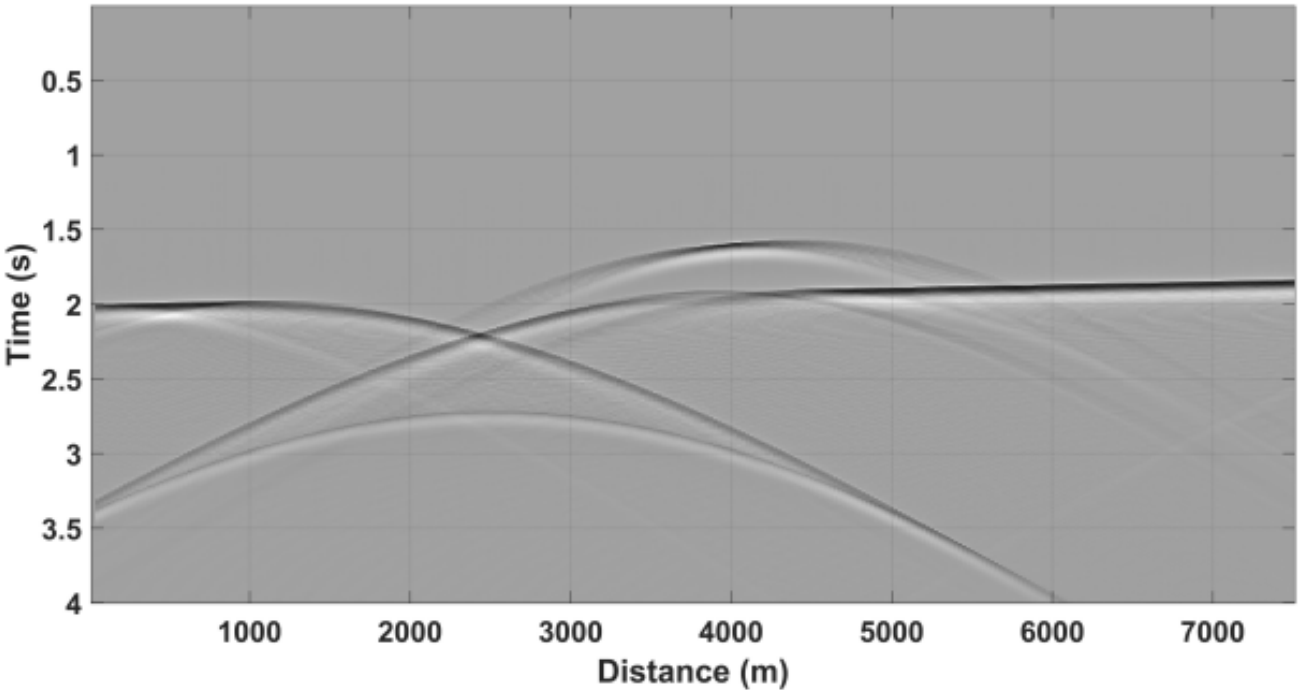


**(b)** A gradient of 0.03 Hz in the $x$-direction is added to the velocity in the layer above the interface.

**Figure 2:** Synthetic common-offset sections ($2h = 50$ m) for the single reflector model. (a) Velocity is constant in the first layer and equal to 2.5 km/s. (b) A gradient of 0.03 Hz in the $x$-direction is added to the velocity in the layer above the interface. In both cases, note the typical bowtie pattern for this kind of model. In case (b), time-skewing in the range of distances 5.0 to 7.5 km is exclusively due to velocity gradient.

For the pre-salt example, we selected an event around $t = 3.5$ s to semi-automatic picking, representative of the top of salt (see Figure 3). Events on the base of salt could have been selected, but these are affected by pull-up effects in regions right under salt domes in the input and time-migrated sections.

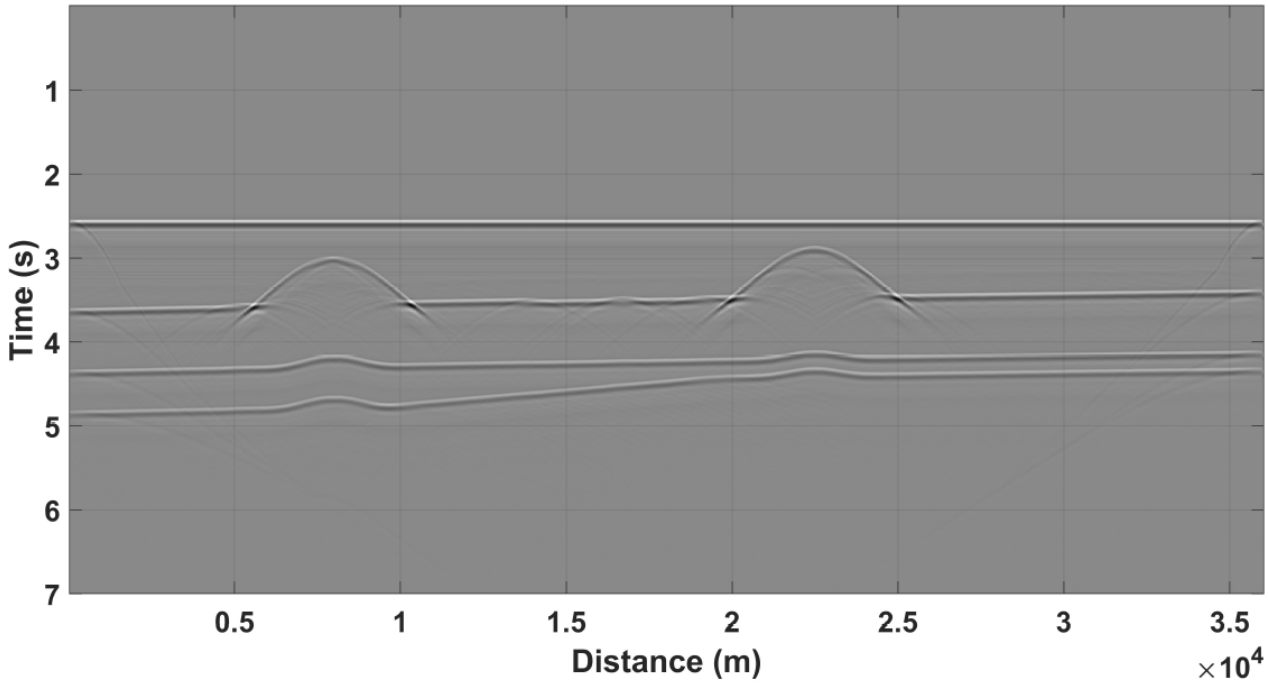


**Figure 3:** Pre-salt model. Common-offset section ($2h = 50$ m) simulating a 2-D seismic marine acquisition over the area of the velocity model defined in Oliveira and Ferreira (2009).

### Time migration

In Figures 4 and 5, the results of the Kirchhoff time migration are seen for the examples of Figures 2 and 3, respectively. Both output sections were previously weighted and migrated accordingly.

The results for unity weight and time remigration are not depicted, since they are essentially the same in terms of structures imaged. Also, the undermigrated time section is not depicted, since only the amplitudes present in the remigrated results are of importance in the comparisons that will be shown in the next section.

## RESULTS AND DISCUSSIONS

### Constant velocity model – single interface

The input dataset for this case is the one depicted in Figure 2a and its time-migrated output section is the one depicted in Figure 4a.

Figure 6 depicts four amplitude profiles picked along the midpoints in Figures 2a (unmigrated) and 4a (time-migrated), as well as along the unity-weight and time-remigrated Kirchhoff equivalent sections (not shown here) for all time samples that eventually show any reflection with peaks at $t = 2$ s. The plot has two vertical scales, to emphasize the fact that the order of magnitudes of the amplitudes in each group of profiles is quite different. The scale of amplitudes on the right refers only to the values of modeling (magenta), while the scale on the left includes amplitudes of unity-weight Kirchhoff time migration (black), true-amplitude weighted-Kirchhoff migration (blue), and Kirchhoff time-remigrated (green diamonds), respectively.

The scaling factors that were multiplied to each picked profile value in each plot are the ones listed in Table 1. Note in Figure 6 that the values of amplitudes after multiplication are proportional and scalable, as initially claimed. The situation is very clear when a laterally continuous range of amplitude values is equal in magnitude. This feature, in the example above, is fair and clearly visible along the range of midpoints 5.0 to 7.0 km.

The order of magnitude for the modeled amplitudes (magenta) in Figure 6 is much lower than the time-migrated and time-remigrated ones, according to the scale of the latter profiles positioned on the left of the plot. It is clear that picked amplitudes after a weighted-Kirchhoff migration (blue) are corrected from geometrical-spreading losses, since they are presented as higher values in relation to migration with unitary weight (black) in the same plot.

As for the time-remigrated amplitudes (green diamonds), they are practically the same as the weighted-Kirchhoff result. In the general approach to seismic imaging of Hubral, Tygel and Schleicher, the cascading of a migration/demigration or a single stack solution grants the best possible amplitudes in a preserving way. For this constant-velocity (and simple) example, this is a faithful statement of this fact.

A final and interesting comparison for the constant velocity example is shown in Figure 7. This time, the black curve of amplitudes along midpoints depicts the picked values for the undermigrated Kirchhoff result, showing that these values of amplitudes are much even higher or overestimated than the

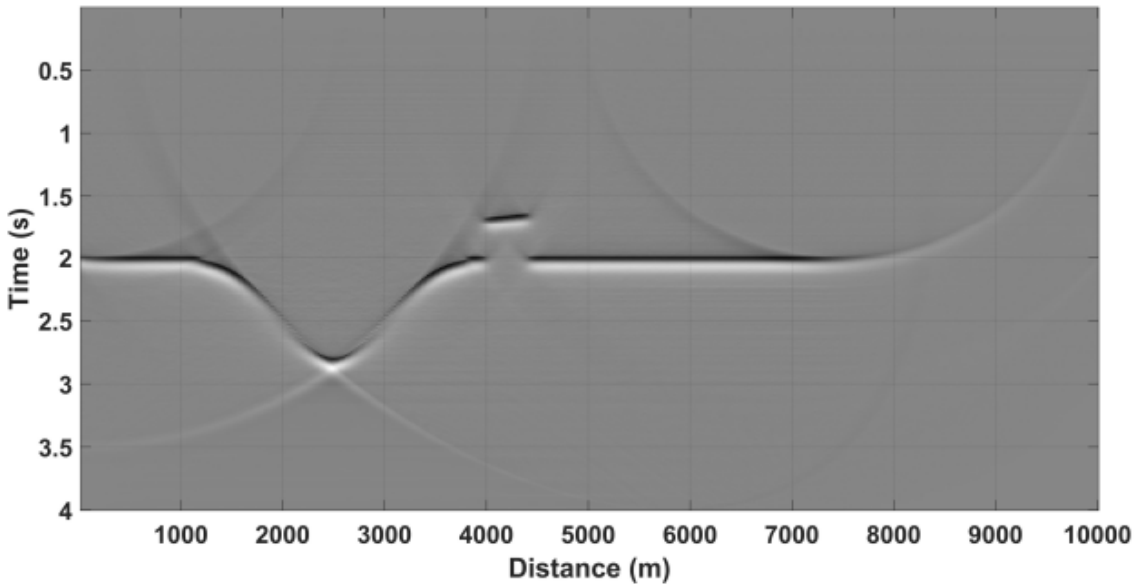


**(a)** Time migration for the constant velocity case.

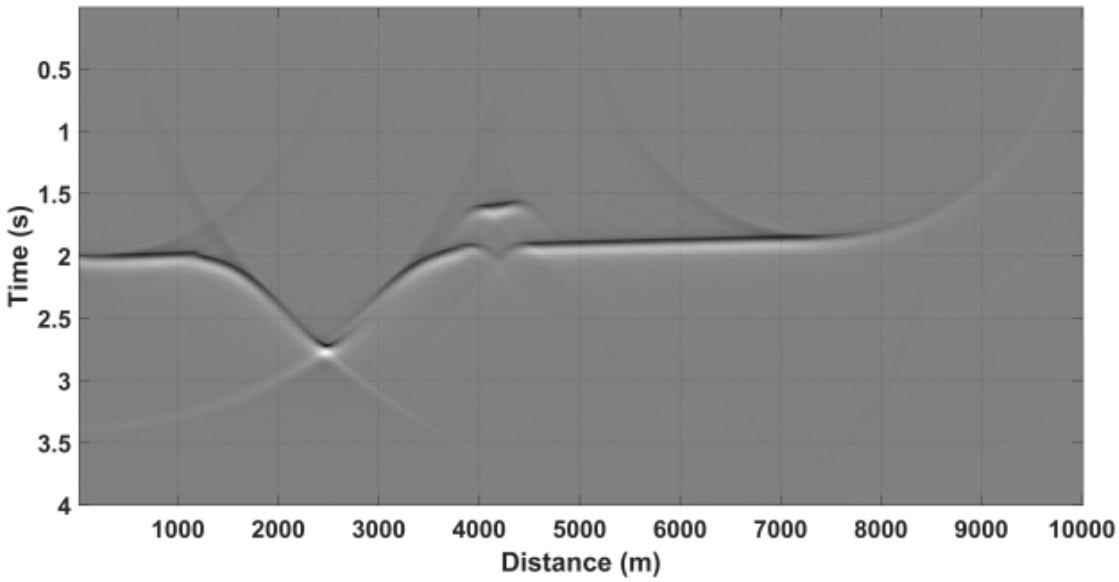


**(b)** Time migration for the gradient case.

**Figure 4:** Time-migrated sections of the input data shown in Figure 2. (a) Constant velocity case. (b) Gradient case.

weighted-Kirchhoff result and, therefore, its amplitudes are not the best possible ones. When these data are time-remigrated, following the lines of Oliveira et al. (2023), the output amplitudes are true again, as predicted in theory (Hubral et al., 1996; Tygel et al., 1996). This again shows that time remigration "pulls" undermigrated amplitudes to their best true-amplitude results.

**Lateral velocity variation – single interface**

When lateral velocity variation is present, time-skewing is one of the features commonly present in time migration (Black and Brzostowski, 1994; Bevc et al., 1995). Figure 2b is a skewed version of the input seismic section for the constant velocity case. Figure 8 then depicts the comparison of picked amplitudes for the same event at $t = 2$ s in the same manner as in Figure 6. This time, the automatic picking for this temporal sample will vary along midpoints, including polarity changes due to skewing. This is an example in which a manual picking should come into play to preserve the lateral continuation of the events being tracked.

Figure 9 then just depicts the same behavior of amplitudes when the true-amplitude results are compared to the undermigrated ones. Again, time remigration "pulls" undermigrated amplitudes to their best true-amplitude results.

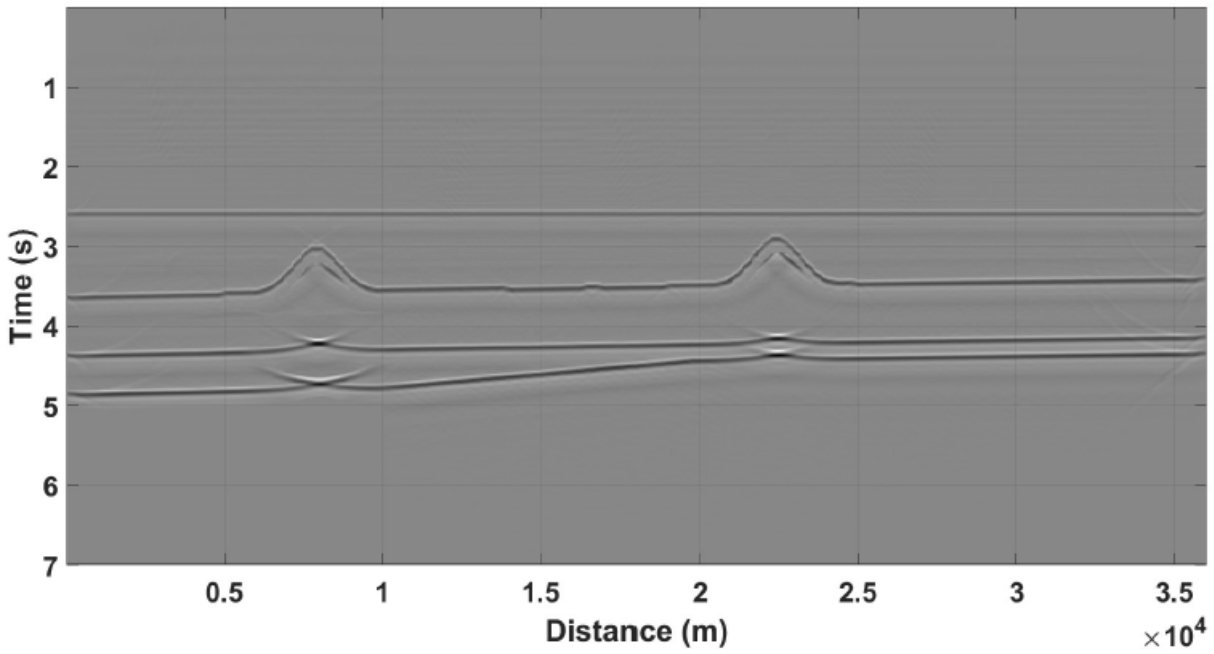


**Figure 5:** Kirchhoff time-migrated seismic section of the input data seen in Figure 3 (pre-salt model). Weighted time migration here presents non-collapsed pull-ups below salt dome events and time-skewing due to lateral velocity gradient.

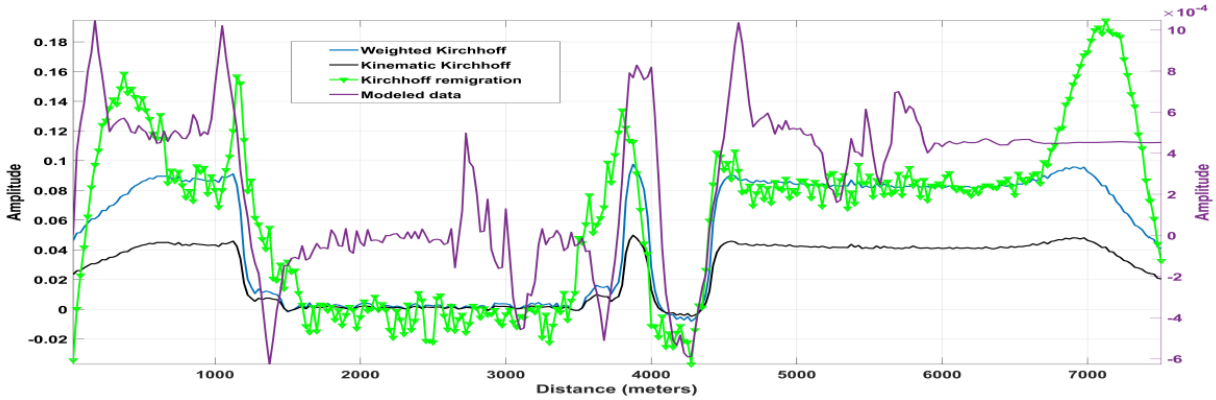


**Figure 6:** Semi-automatically picked amplitudes for an event at $t = 2$ s for the example of constant velocity. See text for details.

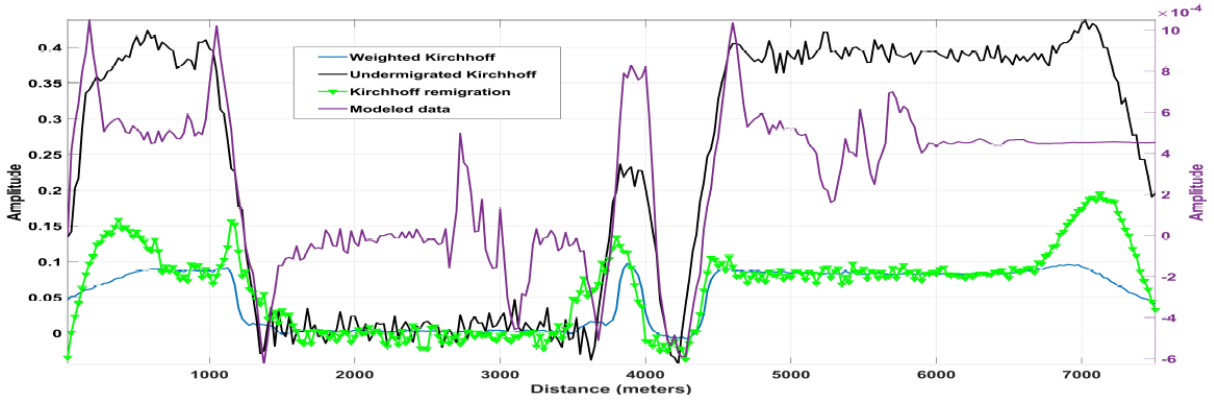


**Figure 7:** Another comparison, as in Figure 6, but this time the black curve shows the values of the undermigrated result when compared to the other true-amplitude ones.

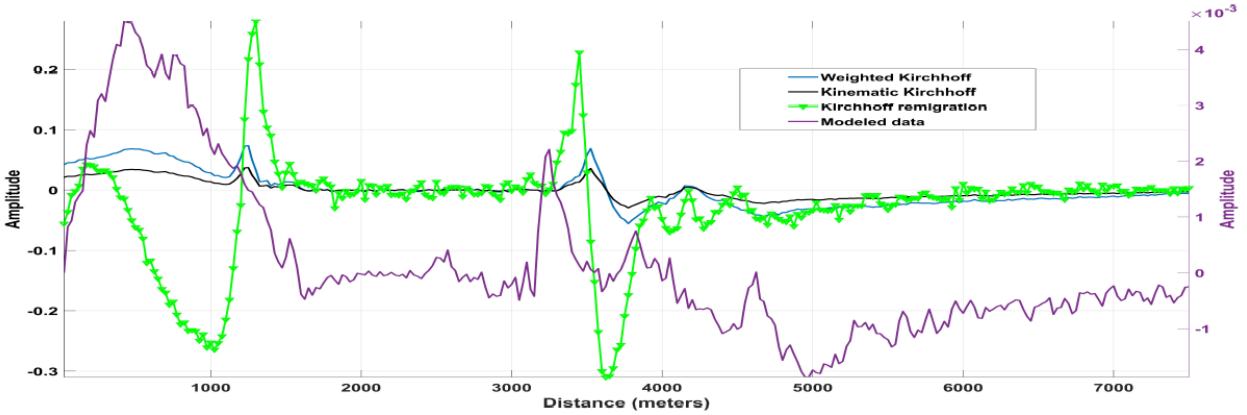


**Figure 8:** Semi-automatically picked amplitudes for an event at $t = 2$ s for the example of lateral velocity variation.

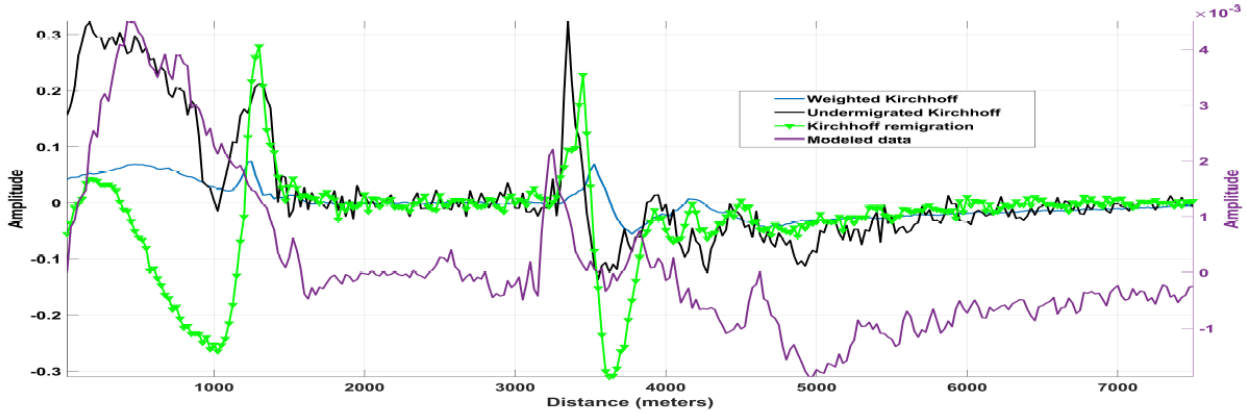


**Figure 9:** Another comparison, as in Figure 8, but this time the black curve shows the values of the undermigrated result when compared to the other true-amplitude ones.

We call attention to the fact that in this latter example, amplitudes were automatically picked, whereas it should have been manually done. But even with the presence of this picking problem, we observe that physically the results are conclusive, agreeing with the one for the constant velocity example.

## Pre-salt model

For this synthetic model of the Brazilian pre-salt (see Figure 1b), the 2.5-D amplitudes were modeled with amplitudes that work as "densities" with dimension equal to $\frac{1}{\sqrt{2}m^{3/2}}$ (see Figure 3). Therefore, any amplitude picked from the reflections of this model must first be scaled with $2\sqrt{dx}$ before any comparison and assessment. The other factors involved in the scaling of picked values for migration and remigration are listed in Table 2.

The picking procedure for this example is the most challenging one. There are several processing issues related to this model. The presence of aliasing noise in modeling and migration seems to contaminate the automatic sample picking in the straightforward manner in which our procedures were done in the previous examples. Our opinion, without proving here, is that a careful manual picking should be mandatory in order to compare all amplitudes, time-migrated or time-remigrated, in a fair way. But since manual picking was not available to us during the writing of this paper, the only solution was to band-pass the data in each of the procedures so as to eliminate as much noise as possible and proceed with semi-automatic picking. Therefore, an Ormsby band-pass filter was applied to the input seismic data before kinematic and weighted migrations, as well as to the undermigrated data before the time remigration procedure. In terms of kinematic imaging, we state that these filtering proved to be quite satisfactory.

Due to these problems, we have chosen two specific time samples of reflection events of the modeled data in order to compare to the same values of picked amplitudes along migrated and remigrated sections (Figure 10). These samples are very close to each other in time and are representative of reflections of the top of the salt layer of the geological model (see Figure 1b). Since the picked events are referred to a single sample in time, the lateral variation of picked values along midpoints in this example shall not follow a continuous trend, but sometimes even oscillate between positive and negative values (change of polarity) due to time-skewing. Notice that, in the areas of the two salt domes (in the range of distances 5 km to 10 km and 20 km to 25 km, respectively; see Figure 5) the picked values for the chosen constant sample must be disregarded, since there are no seismic events there (just noise) and any value picked there

**Table 2:** Pre-salt model contribution to amplitudes.

| Numerical operation | Contribution (dimension) | Amplitude ("density") | Scaling (factor) |
|---|---|---|---|
| Modeling | $\frac{1}{\sqrt{2}}\frac{dx}{m^{3/2}}$ | $\frac{1}{\sqrt{2m}}$ | $\sqrt{2dx}$ |
| Weighted-Kirchhoff | $\frac{1}{\sqrt{2m}}\frac{\sqrt{2s}}{2}\frac{dx}{m}$ | $\frac{1}{2}\sqrt{\frac{s}{m}}$ | $2\sqrt{\frac{dx}{s}}$ |
| Unity-Kirchhoff | $\frac{1}{\sqrt{2m}}\frac{dx}{m}$ | $\frac{1}{\sqrt{2m}}$ | $\sqrt{2dx}$ |
| Remigration | $\frac{\sqrt{2}}{4}\frac{s}{m^2}dx$ | $\frac{\sqrt{2}}{4}\frac{s}{m}$ | $2\frac{\sqrt{2dx}}{s}$ |

must be close to zero in either of the scales used on the following figures. In the case of the input seismic section in these ranges, the picked values are located between two distinctive spikes that indicate the region where edge diffractions of the salt domes occur (see Figure 3).

Figure 10a then depicts the picking profiles for an event located at $t = 3.54$ s. As before, we note an agreement and a proportionality of values in all profiles derived from the modeled (magenta), weighted-Kirchhoff (blue), unity-Kirchhoff (black) and Kirchhoff-remigrated (green) sections. The weighted-Kirchhoff and unity-Kirchhoff follow an equal, proportional and significative trend along the range of distances (and according to their scales), which reflects the fact that their operators perform the same imaging task and adequately locate reflection events, although the derived amplitudes are different in values. This similarity is most noticeable in the range of distances 20 km to 29 km in Figure 10a, but in a general sense the same feature is recognizable along the rest of midpoints. The time-remigrated profile also presents the same feature along all midpoints, but resembles a smoother curve and seems to be affected by some edge effects.

Now let us consider the case of one event located at $t = 3.64$ s. Figure 10b depicts the representative profile section showing the same results as in the previous example. This time, the time-remigrated result (green) is the only profile that presents an distinct behavior, which is negative polarity along most ranges of midpoints. In order to check this proportionality of values with respect to the weighted-Kirchhoff and unity-Kirchhoff, in Figure 10c we have artificially inverted the polarity of the remigrated result. Notice now that the new remigrated profile is most equivalent to the latter ones. Our opinion about this fact is that since time remigration is a weighted-stacking operation, the change of polarity may be associated with some acquired complex phase due to its weight function.

As a final example for this pre-salt model, Figure 10d depicts a careful picking of values of the top of salt reflections (again, considering reflections under the domes to be near zero). This time, an initial time at $t = 3.588$ s is selected as a linear coefficient for a straight line direction following a specific angular coefficient, corresponding to the top of salt reflections that are skewed upwards in time. The picking under theses conditions is still automatic, but now follows a more oriented direction and as close as possible of an example of a manual picking. Then, Figure 10d depicts the fact that all profiles present a common morphology; the only difference is the scale and proportion of picked values. This last example proves our claim that manual picking procedure provides straightforward and meaningful results.

As before, it must be noticed that the picked time-migrated and time-remigrated amplitudes are proportional to the ones from the input seismic data, according to their respective scales, after the use of the scaling factors listed in Table 2. Also, it is important to notice that, in all examples, the remigrated picked values follow closely and proportionally the weighted-Kirchhoff values, as already shown in previous examples and theoretical predictions (Hubral et al., 1996; Tygel et al., 1996).

## CONCLUSIONS

We have successfully studied the scaling of amplitudes derived from weighted time migration and time remigration processes and their comparison to scaled amplitudes picked along modeled seismic data. In this study, we have made use of 2-D synthetic data only.

Recognizing that numerically modeled 2.5-D amplitudes work as “densities” (i.e., they are physical constants), we have devised some scale factors for modeling, migration and remigration that make amplitudes dimensionless. When these factors are directly multiplied to picked amplitude values of reflection events, the magnitude of each event is equalized and the scales of their values become proportional. Following this reasoning, we have shown ad hoc that picked time-migrated and time-remigrated amplitudes (i.e., corrected for geometrical spreading) are also proportional to amplitudes picked from their input seismic data in a true sense (Schleicher et al., 1993).

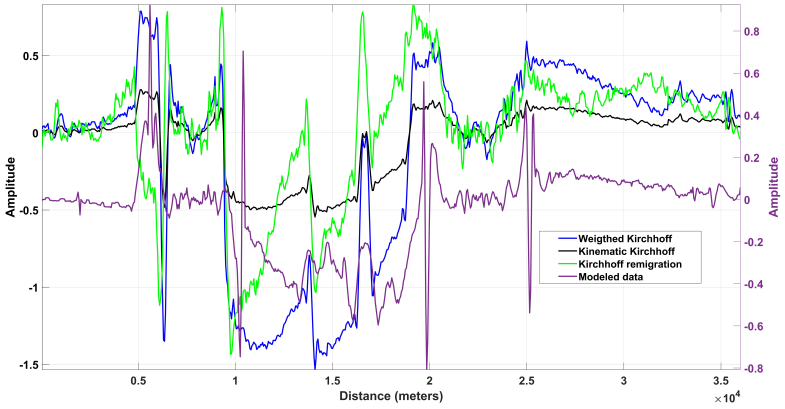


**(a)** Event at $t = 3.54$ s.

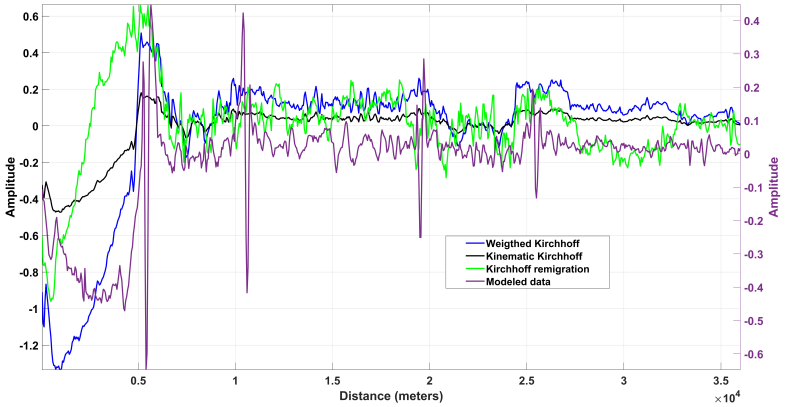


**(b)** Event at $t = 3.64$ s. Negative polarity (remigration).

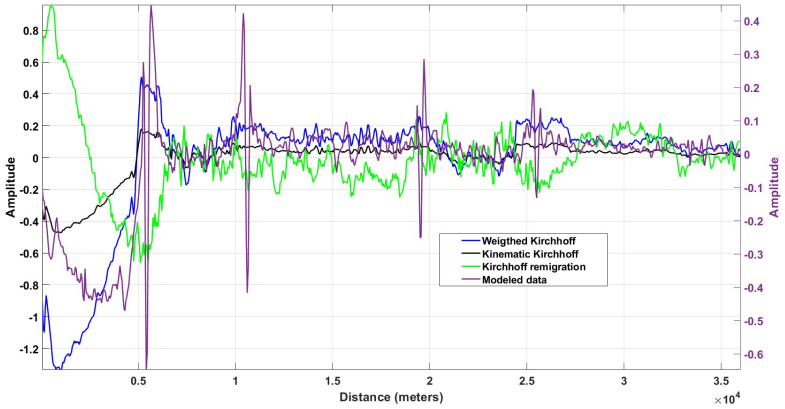


**(c)** Event at $t = 3.64$ s. Positive polarity (remigration).

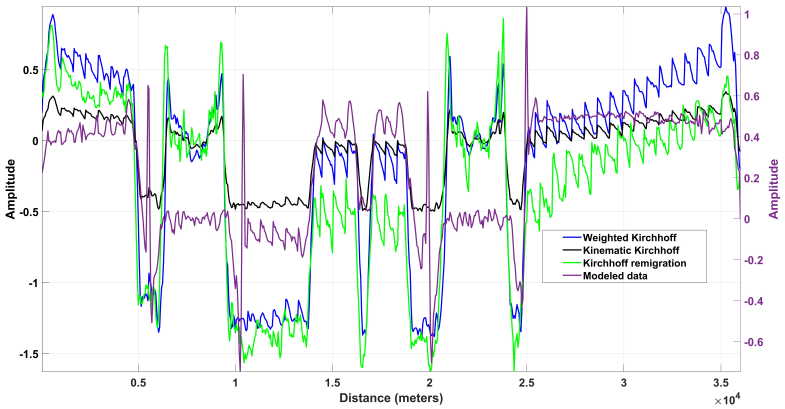


**(d)** Event at $t = 3.588$ s. This time all amplitudes were picked along a linear trend at the base of salt.

**Figure 10:** Picked amplitudes for events at 3.54 s, 3.64 s and 3.588 s, representative of the top of the salt layer.

We have tested the present procedure in two synthetic, common-offset, 2.5-D seismic dataset. The input dataset of the first model considers only an interface separating two media, where, for the first layer, cases of constant velocity and initial velocity with lateral variation along the $x$-direction were accounted for. The input dataset of the second model is representative of a 2-D marine acquisition over a regional pre-salt area derived from any of the Brazilian East Margin offshore basins (Oliveira and Ferreira, 2009), including lateral velocity variations in the Cretaceous and SAG/rift sections. In both cases, each input seismic section was then time-migrated using a weighted-Kirchhoff (Schleicher et al., 1993) and an unity-Kirchhoff algorithm to provide the main migrated sections containing reflection horizons that may be used for picking. In order to generate input data to the remigration procedure in the time domain (Oliveira et al., 2023), we have also generated weighted-undermigrated results using the same algorithm. These additional imaging results are not shown here, just their picked values.

The results obtained in all examples showed that the scaling of amplitudes by dimensional factors is capable of equalizing magnitudes of the picked events, at least proportionally, increasing the confidence of their physical interpretation.

## ACKNOWLEDGMENTS

The first author would like to thank ANP/RJ and ANM/MT for the permission to take part in this work. The last author would like to thank CNPQ for his MSc scholarship, during all the stages of this research.

## DATA AND MATERIALS AVAILABILITY

The data used in the manuscript is open and publicly available whenever possible.

The source codes are available for downloading at: https://github.com/alexfisic/2.5-D-seismic-remigration.

## APPENDIX A. KIRCHHOFF-TYPE REMIGRATION THEORY

In this appendix we present a brief description of the remigration theory (Hubral et al., 1996; Tygel et al., 1996), considering its counterpart in the time domain (Oliveira et al., 2023).

Similar to the Kirchhoff-type theory described in Tygel et al. (1998) and Schleicher and Bagaini (2004), for each point $(\tilde{x},\tilde{\tau})$ in the output time-remigrated section to be simulated, the stack result $\tilde{I}(\tilde{x},\tilde{\tau})$ is obtained by a weighted stack of the input data, represented by the following integral

$$\tilde{I}(\tilde{x},\tilde{\tau}) = \frac{1}{\sqrt{2\pi}} \int_A dx\, K_{RM}^{(2.5D)}(x;\tilde{x},\tilde{\tau}) \times \partial_\tau^{1/2} I(x,\tau)\big|_{\tau=t_{RM}(x;\tilde{x},\tilde{\tau})}. \tag{A1}$$

where $I(x,\tau)$ is the input time-migrated (analytic) seismic section that is to be weighted by $K_{RM}^{(2.5D)}(x;\tilde{x},\tilde{\tau})$ and then summed up along the stacking line or inplanat $\tau = t_{RM}(x;\tilde{x},\tilde{\tau})$ (Tygel et al., 1996). The time-reverse generic half-derivative

$$\partial_{-t}^{1/2}[f(t)] = \frac{1}{\sqrt{2\pi}} \int_{-\infty}^{+\infty} d\omega\, |\omega|^{1/2} e^{-i\frac{\pi}{4}\,\mathrm{sign}(\omega)} \times F(\omega)\, e^{-i\omega t}. \tag{A2}$$

is applied to input traces in order to correct the pulse shape. Here, $f(t)$ is any function of its argument.

In inhomogeneous medium and considering the presence of mild lateral velocity variation, for a finite-offset ($2h$) configuration, the stacking line for the remigration procedure is given by Equation (A3) (Martins, 2001):

$$t_{RM}^{(\xi)}(x;\tilde{x},\tilde{\tau}) = \sqrt{\tilde{\tau}_D^2 - \frac{4h^2}{v_{RMS}^2}}\sqrt{1 - \frac{(x-\xi^*(x))^2}{\frac{v_{RMS}^2}{4}\tilde{\tau}_D^2}}. \tag{A3}$$

In (A3), $\tilde{\tau}_D$ is the diffraction traveltime for coordinate $(\tilde{x},\tilde{\tau})$ in the output space, represented by two DSRs for two branches of the traveltime to the image point, wherein velocity $\tilde{v}_{RMS}$ is used relative for each source and geophone in that domain. Here, the stationary value $\xi^*(x)$ is the coordinate that relates the inplanat $\tau = t_{RM}(x;\tilde{x},\tilde{\tau})$ with its respective coordinates in the input and output domains (Tygel et al., 1996).

Two conditions constrain the aperture $A$ range for time remigration following Equation (A3). The first is offset-dependent (i.e., $\tilde{\tau}_D^2 > 4h^2/v_{RMS}^2$), which means that, in all offsets, very shallow to shallow events (whenever they are recorded) must be disregarded or are not imaged around any stationary value $\xi^*(x)$ that may exist along these shallow time intervals. The second constraint is related to the condition $(x-\xi^*(x))^2 < \frac{v_{RMS}^2}{4}\tilde{\tau}_D^2$, which restricts the number of traces to be stacked around the stationary value $\xi^*(x)$.

The remigration weight function for the numerical procedure – see Equation (1) of the main text – is given by the direct multiplication of two weight functions (migration and demigration). Another simplification of the same weight function is obtained when it is replaced by a pseudo-depth or time domain version proportional to the so-called Beylkin determinant (Martins et al., 1997), dimensionally equivalent to its

depth version. In 2.5-D, the Beylkin determinant in depth is reduced to a form that is proportional to a 2-D version, because in this case the 2.5-D migration weight function is defined in terms of this determinant and other ray theory elements (i.e., product of geometrical spreadings for each source and receiver ray branch) as the 2.5-D demigration weight function is proportional to the reciprocal of the products of the geometrical-spreadings (Martins, 2001). Since in remigration there is numerical multiplication of migration/demigration weight functions, there is an explicit possibility that these geometrical-spreading terms cancel each other when a stationarity condition holds (Tygel et al., 1996).

A special computer code was written in order to use the cascaded remigration operator with a weight function proportional to the Beylkin determinant, $\tilde{h}_B^{(2D)}(\xi;\tilde{M})$, in the time domain (see Appendix B). As a result, and considering that at the image condition during migration ($t=0$) there will be stationarity, the product of the migration/demigration weight functions will have the following format:

$$K_{RM}^{(2.5D)}(x;\tilde{x},\tilde{\tau}) = \tilde{K}_{DS}^{(2.5D)}(\xi;\tilde{M}) K_{IS}^{(2.5D)}(x;N) = \frac{v_{RMS}^{3/2}}{4}\,\tilde{h}_B^{(2D)}(\xi;\tilde{M})\sqrt{m_D(x)}. \tag{A4}$$

where $\tilde{M} = \tilde{M}(\tilde{x},\tilde{\tau})$ and $N = N(x,\tau)$ are locations in the input and output spaces, respectively. The function $m_D(x)$ is the stretch factor defined in Tygel et al. (1994). It is important to specify that to all examples followed in this paper, the meaning of $v_{RMS} = v_{RMS}(\tilde{x},\tilde{\tau})$ is mandatory and assumed a priori.

Considering this new notation, the final stacking integral of the numeric chained process shall have the following form:

$$\tilde{I}(\tilde{x},\tilde{\tau}) = \frac{1}{\sqrt{2\pi}} \iint_A d\xi\, dx\, K_{RM}^{(2.5D)}(x;\tilde{x},\tilde{\tau}) \times \frac{d}{d\tau} I(x,\tau)\Big|_{\tau=t_{RM}^{(\xi)}(x;\tilde{x},\tilde{\tau})}. \tag{A5}$$

It must be emphasized that the double integral in Equation (A5) refers to a 2-D process and that it is a one-step chained migration/demigration procedure.

## APPENDIX B. THE BEYLKIN DETERMINANT IN THE TIME DOMAIN

In equation (A4), the so-called 2-D Beylkin determinant $\tilde{h}_B^{(2D)}(\xi;\tilde{M})$ must be evaluated in pseudo-depth, where generically $z = vt/2$. Thus, it is defined:

$$\tilde{h}_B^{(2D)}(\xi;\tilde{M}) = det\begin{pmatrix} \frac{\partial\tilde{\tau}_D(\xi;\tilde{M})}{\partial\tilde{x}} & \frac{2}{\tilde{v}_{RMS}}\frac{\partial\tilde{\tau}_D(\xi;\tilde{M})}{\partial\tilde{\tau}} \\ \frac{\partial^2\tilde{\tau}_D(\xi;\tilde{M})}{\partial\xi\partial\tilde{x}} & \frac{2}{\tilde{v}_{RMS}}\frac{\partial^2\tilde{\tau}_D(\xi;\tilde{M})}{\partial\xi\partial\tilde{\tau}} \end{pmatrix}. \tag{B6}$$

In this appendix let us study the explicit form of this function, which is part of the weight function in Equation (A5) used in some cases in this paper.

Let the first row of the Beylkin determinant be given by the following elements

$$B_{11} = \frac{\partial\tilde{\tau}_D}{\partial\tilde{x}} = \frac{1}{\tilde{v}_{RMS}^2}\left[\frac{(\tilde{x}-\xi-h)}{\tilde{t}_S} + \frac{(\tilde{x}-\xi+h)}{\tilde{t}_G}\right] \tag{B7}$$

and

$$B_{12} = \frac{2}{\tilde{v}_{RMS}}\frac{\partial\tilde{\tau}_D}{\partial\tilde{\tau}} = \frac{\tilde{\tau}}{2\tilde{v}_{RMS}}\left(\frac{1}{\tilde{t}_S}+\frac{1}{\tilde{t}_G}\right). \tag{B8}$$

Here, $\tilde{t}_S$ and $\tilde{t}_G$ are traveltime branches of the double-square-root equation for the diffraction point $(\tilde{x},\tilde{\tau})$ in the output space, whereas $\tilde{v}_{RMS}$ is its respective stacking velocity.

The second row of the matrix presents the following elements

$$B_{21} = \frac{\partial^2\tilde{\tau}_D}{\partial\xi\,\partial\tilde{x}} = -\frac{1}{\tilde{v}_{RMS}^2}\left(\frac{1}{\tilde{t}_S}+\frac{1}{\tilde{t}_G}\right) + \frac{(\tilde{x}-\xi-h)^2}{\tilde{t}_S^3\,\tilde{v}_{RMS}^4} + \frac{(\tilde{x}-\xi+h)^2}{\tilde{t}_G^3\,\tilde{v}_{RMS}^4}. \tag{B9}$$

and

$$B_{22} = \frac{2}{\tilde{v}_{RMS}}\frac{\partial^2\tilde{\tau}_D}{\partial\xi\,\partial\tilde{\tau}} = \frac{\tilde{\tau}}{2\,\tilde{v}_{RMS}^3}\left[\frac{\tilde{x}-\xi-h}{\tilde{t}_S^3}+\frac{\tilde{x}-\xi+h}{\tilde{t}_G^3}\right]. \tag{B10}$$

Therefore, all elements of the Beylkin determinant described above are expressed as functions of traveltimes and other parameters related to seismic acquisition (source-geophone pair coordinates, parameterized by midpoints and half-offset), besides output space coordinates and RMS stacking velocities. Then, in numerical implementations of equation (A5), one just have to do $\tilde{h}_B^{(2D)}(\xi;\tilde{M}) = B_{11}B_{22} - B_{12}B_{21}$ in order to calculate the Beylkin determinant.

Finally, it is important to state that, dimensionally, $[\tilde{h}_B^{(2D)}(\xi;\tilde{M})] = [\frac{s^2}{m^3}]$. This dimension is equivalent to the one of the Beylkin determinant in the depth domain.

## REFERENCES


Bevc, D., J. L. Black, and G. Palacharla, 1995, Plumes: Response of time migration to lateral velocity variation: Geophysics, **60**, 1118–1127, doi: 10.1190/1.1443840.

Black, J. L., and M. A. Brzostowski, 1994, Systematics of time-migration errors: Geophysics, **59**, 1419–1434, doi: 10.1190/1.1443699.

Bleistein, N., 1986, Two-and-one-half dimensional in-plane wave propagation: Geophysical Prospecting, **34**, 686–703, doi: 10.1111/j.1365-2478.1986.tb00488.x.

Fomel, S., 2003, Velocity continuation and the anatomy of residual prestack time migration: Geophysics, **68**, 1650–1661, doi: 10.1190/1.1620639.

Hubral, P., J. Schleicher, and M. Tygel, 1996, A unified approach to 3-D seismic reflection imaging, part I: Basic concepts: Geophysics, **61**, 742–758, doi: 10.1111/j.1365-246X.1996.tb00009.x.

Martins, J., J. Schleicher, M. Tygel, and L. Santos, 1997, 2.5-D true-amplitude Kirchhoff migration and demigration: Journal of Seismic Exploration, **6**, 159–180, doi: 0963-0651/97.

Martins, J. L., 2001, Migração, demigração e imageamento em 2.5D com inclusão de alguns casos analíticos: PhD thesis, 107p. UNICAMP, Campinas-SP.

O'Doherty, R., and N. A. Anstey, 1971, Reflections on amplitudes: Geophysical Prospecting, **19**, 430–458, doi: 10.1111/j.1365-2478.1971.tb00610.x.

Oliveira, A. D. S., and C. A. S. Ferreira, 2009, Modeling of a synthetic presalt 2-D seismic dataset representative of offshore East margin basins (Brazil)–preliminary results: Presented at the 11th International Congress of the Brazilian Geophysical Society. doi: 10.1190/sbgf2009-300.

Oliveira, A. D. S., C. A. S. Ferreira, and J. Lourenço, 2023, Kirchhoff time-remigration and time-to-depth conversion – preliminar studies and possible applications: Presented at the 18th International Congress of the Brazilian Geophysical Society.

Schleicher, J., and C. Bagaini, 2004, Controlling amplitudes in 2.5-D common-shot migration to zero offset: Geophysics, **69**, 1299–1310, doi: 10.1190/1.1801946.

Schleicher, J., M. Tygel, and P. Hubral, 1993, 3-D true-amplitude finite-offset migration: Geophysics, **58**, 1112–1126, doi: 10.1190/1.1443495.

Sheriff, R. E., 1975, Factors affecting seismic amplitudes: Geophysical Prospecting, **23**, 125–138, doi: 10.1111/j.1365-2478.1975.tb00685.x.

Tygel, M., J. Schleicher, and P. Hubral, 1994, Pulse distortion in depth migration: Geophysics, **59**, 1561–1569, doi: 10.1190/1.1443545.

Tygel, M., J. Schleicher, and P. Hubral, 1996, A unified approach to 3-D seismic reflection imaging, part II: Theory: Geophysics, **61**, 759–775, doi: 10.1190/1.1444002.

Tygel, M., J. Schleicher, P. Hubral, and C. Hanitzsch, 1993, Multiple weights in diffraction stack migration: Geophysics, **58**, 1820–1830, doi: 10.1190/1.1443397.

Tygel, M., J. Schleicher, P. Hubral, and L. T. Santos, 1998, 2.5-D true-amplitude Kirchhoff migration to zero offset in laterally inhomogeneous media: Geophysics, **63**, 557–573, doi: 10.1190/1.1444356.


**Carlos A. S. Ferreira**: Conceptualization (lead), Methodology (lead); Software (lead), Validation (lead), Formal analysis (lead), Resources (supporting), Data curation (supporting), Writing - original draft (lead), Writing – review and editing (lead), Visualization (lead), Supervision (lead), Project administration (supporting), Funding acquisition (supporting); **Karina P. Gomes**: Conceptualization (lead), Methodology (lead), Software (lead), Validation (lead), Formal analysis (supporting), Resources (lead), Data curation (lead), Writing - original draft (lead), Writing – review and editing (lead), Visualization (supporting), Supervision (supporting), Project administration (supporting), Funding acquisition (lead); **Alexandre S. Oliveira**: Conceptualization (supporting), Methodology (supporting), Software (lead), Validation (lead), Formal analysis (supporting), Resources (lead), Data curation (lead), Writing - original draft (supporting), Writing – review and editing (lead), Visualization (lead), Supervision (lead), Project administration (lead), Funding acquisition (lead).

Received on December 21, 2023 / Accepted on July 20, 2024